Journal of Advanced Research 43 (2023) 73–85

Contents lists available at ScienceDirect

Journal of Advanced Research

journal homepage: www.elsevier.com/locate/jare

Original Article

Visually predicting microRNA-regulated tumor metastasis by intracellularly 3D counting of fluorescent spots based on *in situ* growth of DNA flares

Chang Xue [a], Huimin Niu [a,b], Shuyao Hu [a], Zhe Yang [a], Lei Wang [a,c], Zai-Sheng Wu [a,*]

[a] *Cancer Metastasis Alert and Prevention Center, Fujian Provincial Key Laboratory of Cancer Metastasis Chemoprevention and Chemotherapy, Pharmaceutical Photocatalysis of State Key Laboratory of Photocatalysis on Energy and Environment, College of Chemistry, Fuzhou University, Fuzhou 350108, China*
[b] *Fujian Key Laboratory of Aptamers Technology, The 900th Hospital of Joint Logistics Support Force, Fuzhou 350025, China*
[c] *Hunan Provincial Key Laboratory of Phytohormones and Growth Development, College of Bioscience and Biotechnology, Hunan Agricultural University, Changsha 410128, China*

HIGHLIGHTS

- An intracellular *in situ* growth of optical DNA flares, grid-patterned DNA-protein hybrids (GDPHs).
- GDPH flares are nuclease-resistant and discrete objects with retarded mobility for *in situ* and accurate counting of miRNA
- The cancer metastasis in murine tumor models is predicted by counting intracellular GDPH flares.

GRAPHICAL ABSTRACT

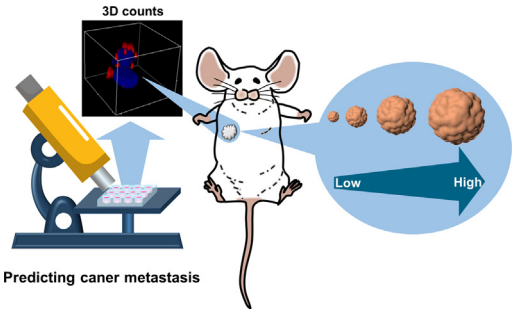

ARTICLE INFO

Article history:
Received 2 August 2021
Revised 2 January 2022
Accepted 1 March 2022
Available online 4 March 2022

Keywords:
Grid-patterned DNA-protein hybrid (GDPH)
Three-dimensionally (3D) fluorescence counts
miR-21
Cell viability
Prevention of cancer metastasis

ABSTRACT

Introduction: MicroRNAs (miRNAs) have been revealed to be critical genetic regulators in various physiological processes and thus quantitative information on the expression level of critical miRNAs has important implications for the initiation and development of human diseases, including cancers.
Objectives: We herein develop three-dimensionally (3D) counting of intracellular fluorescent spots for accurately evaluating microRNA-21 (miRNA-21) expression in individual HeLa cells based on stimuli-activated *in situ* growth of optical DNA flares, grid-patterned DNA-protein hybrids (GDPHs).
Methods: Target miRNA is sequence-specifically detected down to 10 pM owing to efficient signal amplification. Within living cells, GDPH flares are nuclease resistant and discrete objects with retarded mobility, enabling the screening of intracellular location and distribution of miRNAs and realizing *in situ* counting of target species with a high accuracy.
Results: The quantitative results of intracellular miRNAs by 3D fluorescence counts are consistent with qPCR gold standard assay, exhibiting the superiority over 2D counts. By screening the expression of

Abbreviations: 1D, One-dimensional; 2D, Two-dimensional; 3D, Three-dimensional; GDPHs, Grid-patterned DNA-protein hybrids; qPCR, Quantitative polymerase chain reaction; PDCD4, Programmed cell death 4 protein; CTCs, Circulating tumor cells; RNA, Ribonucleic acid; DNA, Deoxyribonucleic acid; 3D-IFC, 3D counting of intracellular fluorescent spots; BPMB, Biotinylated palindromic molecule beacon; A-BPMB, trivalent target-recognition probe; eSDR, Enzymatic strand displacement reaction; FSs, Fluorescent spots; ^{C}SDA, Cross-linking strand displacement amplification; ds, Double-stranded; KFP, Klenow fragment polymerase (3′-5′exo-); dNTPs, deoxyribonucleotides; Lipo2000, Lipofectamine 2000; PMSF, Phenylmethanesulfonyl fluoride; FBS, Fetal bovine serum; v-DT, 'visible' DNA target molecule; NC, Nitrocellulose; GAPDH, Glyceraldehyde-3-phosphate dehydrogenase; CCK8, Cell Counting Kit-8; AFM, Atomic force microscopy; SA, Streptavidin; LDP, Linear DNA products; ^{L}SDA, Strand displacement amplification with LDP as products; LOD, Limit of detection; AIM, Apparent intracellular mobility; MCC, Manders' colocalization coefficients; PRC, Pearson's correlation coefficient; RCG, relative cell growth; PI, Propidium iodide; NE, Normalized expression; RFU, Relative fluorescence units; e-miR-21, Exogenous miR-21 mimics.

Peer review under responsibility of Cairo University.

* Corresponding author.
E-mail address: wuzaisheng@163.com (Z.-S. Wu).

https://doi.org/10.1016/j.jare.2022.03.001

intracellular miR-21 that can down-regulate the programmed cell death 4 (PDCD4) protein, the proliferation and migration of HeLa cells, including artificially-regulated ones, were well estimated, thus enabling the prediction of cancer metastasis in murine tumor models.
Conclusion: The experiments *in vitro*, *ex vivo* and *in vivo* demonstrate that GDPH-based 3D fluorescence counts at the single cell level provide a valuable molecular tool for understanding biological function of miRNAs and especially for recognizing aggressive CTCs, offering a design blueprint for further expansion of DNA structural nanotechnology in predicting distant metastasis and prevention of tumor recurrence after primary resection.

Introduction

It is well-known that malignant tumor (cancer) is an important public health problem all over the world. At present the incidence and mortality rates of cancer are still very high, especially in the developing world. Disseminated cancers are the main causes of death in patients with tumors, which is considered to be determined by circulating tumor cells (CTCs) detaching from the primary tumors and homing in various distant organs via the blood circulation systems [1]. Therefore, evaluation of the malignant potential (often associated with critical molecular events, for example, the aberrant expression of miRNAs and functional proteins) of CTCs is of significant importance for the prediction of tumor metastasis and prevention of the recurrence after primary resection.

Nucleic acids and proteins are two indispensable constituents of living organisms with different roles. The main functions of nucleic acids are to provide the recipe to the cells for the protein synthesis [2], while proteins paly a fundamental role for most biological processes [3]. The interaction between proteins and nucleic acids often plays a necessary role in various biological events [4]. Since the first discovery in nematodes, small non-coding RNA species (miRNAs) have been revealed as the critical regulators in numerous biological processes [5], such as cell differentiation, proliferation and apoptosis [6,7]. The abnormal expression of miRNAs often causes a variety of human diseases [8], and the miRNA-involved regulatory processes of functional proteins are considered to be valuable tools for uncovering basic biological mechanism of the initiation and progression of diseases. Because the genetic instability leads to the tumor cell heterogeneity, the copy number of miRNAs varies from cell to cell even at various stages of cell cycle in the same population [9]. Thus, it is of practical clinical importance to detect the expression profile of tumor-associated miRNAs in individual cells. However, it is extremely difficult for the existing methods to detect intracellular miRNAs due to the complexity of intracellular environment that contains a multitude of interfering factors and functional biomolecules (e.g., nucleases with high digestion ability) capable of potentially preventing or quenching the signaling process [10]. Moreover, the intrinsic molecular characteristics of miRNAs (i.e., small size, sequence homology among family members and low abundance) make their accurate detection more challenging [11]. In view of the desirable ability of fluorescence microscopy to map the spatial distribution of optical molecules, to promote the miRNA-related clinical theranostics, considerable amount of impressive works have been devoted to the development of a variety of imaging methods to extract the biological information on intracellular miRNAs in living cells [12]. Despite some recent important advances in intracellular bioimaging [13], until now there is no report on a well-established signaling platform that allows the precise positioning of intracellular miRNAs in three-dimensional (3D) space in individual cells in a quantitative manner because of a formidable technical obstacle.

To break through the existing bottleneck of 3D spatial quantification of biomolecules in individual cells, herein we demonstrate 3D counting of intracellular fluorescent spots that are enzymatically *in situ* assembled from DNA probes in a stimuli-responsive fashion. When designing a mapping scheme, the following several issues need to be taken into account: (i) *In situ* signaling. Reporting probes could specifically assemble into the architecture of appropriated size with very low mobility so that it remains where it is originally formed. (ii) High nuclease-degradation resistance. To increase the lifetime of signaling probes in complex intracellular environment, DNA assemblies should have the enhanced structural rigidity to protect probe components from nuclease attack [14]. (iii) Signal amplification of individual binding events. To improve the detection sensitivity of fluorescent probe, the probe should be elaborately designed so that one target binding event enables many probes to fluoresce, producing an amplified signal output. Moreover, the signal is required to be on an individual rather than collective level to count the number of miRNAs. (iv) Controlled assembly. To form the countable fluorescent flares, the outgrowth of DNA products should be limited to produce discrete architectures. Moreover, to screen the intact cell behavior for unique purposes, such as accurate evaluation of cell proliferation for predicting malignant invasion of tumor cells, the detection probes should have high biocompatibility so that they do not induce cell damage. Besides, designers should strive to arrange multiple recognition sites in one detection probe and employ a very small number of probe types to increase the local concentration of recognition site. To meet these requirements, the current 3D counting of intracellular fluorescent spots (3D-IFC) is based on intracellular *in situ* growth of grid-patterned DNA-protein hybrid (GDPH) from streptavidin/biotin interaction-mediated trivalent target-recognizing probes by enzymatic strand displacement reaction-based DNA structural nanotechnology.

DNA structural nanotechnology has been used to develop various sophisticated nanostructures, including one-dimensional (1D) [15], two-dimensional (2D) [16] and three-dimensional (3D) architectures [17]. Besides good biocompatibility, structural programmability, vast sequence design space and easy functionalization [18], 2D DNA nanoarrays have been demonstrated to have high stability in contrast to common nucleic acids such as natural, single- and double-stranded DNA [19], which is desirable for *in vivo* applications. Moreover, due to the large steric hindrance originating from the high surface-area-to-volume ratio, grid DNA array is proved to exhibit extremely low mobility [20]. Thus, 2D DNA nanostructure is attractive alternative material for the *in situ* imaging of subcellular location and distribution of biomolecules of interest. Moreover, a rich variety of enzymes are available for providing the powerful "toolbox" for manipulating DNA assemblies, further expanding the area of DNA nanotechnology. Besides, the artificial DNA-protein conjugates with high affinity constant, such as streptavidin/biotinylated DNA complex, offer unique opportunities for constructing well-defined DNA nanostructures

[21]. Nevertheless, while 1D and 3D DNA nanostructures are extensively employed in biosensing, bioimaging and other biomedical applications [22,23], the *in vivo* application of 2D grid-patterned DNA assemblies is largely unexplored. Moreover, the previously-reported DNA nanotechnologies for the assembly of 1D and 3D architectures seem to be unsuitable for the 3D-IFC-based assay of miRNAs within living cells.

On the basis of the above considerations, to perform 3D-IFC-based assay of miRNAs, trivalent target-recognition probe (A-BPMB) is prepared by utilizing streptavidin to glue three biotinylated palindromic molecule beacon (BPMB) together. After transfecting A-BPMB into target cells, enzymatic strand displacement reaction (eSDR) occurs upon intracellular miRNAs and promotes the intermolecular cross-linking among different A-BPMBs, enabling the *in situ* growth of 2D discrete GDPH nanosheet flares (fluorescent spots, FSs) that can be detected in a target-specific-amplification manner. Introduction of palindromic end into MB probes make them hybridize with each other, simplifying the probe design. Each A-BPMB has three binding sites for target miRNAs, increasing their collision probability. In view of the target recycle-based signal amplification and cross-linking effect, eSDR is called the cross-linking strand displacement amplification (^{C}SDA) capable of assisting the intermolecular double-stranded (ds) DNAs to assemble into highly cross-linked network structure. By fluorescently counting the number of FSs and visualizing their location in three-dimensional space, the expression level of target miRNAs and subcellular distribution can be estimated in individual cells. By utilizing GDPH-based 3D-IFC technique, we quantitatively evaluate the proliferation of tumor cells and in turn predict the tumorigenesis and assess the response of preventive therapeutic intervention. The experimental data *in vitro* and *in vivo*, including the results from tumor-bearing nude mice model, demonstrate the potential application of GDPH–based 3D-IFC technique in the molecular diagnosis and prevention of cancers.

Methods

Materials

All oligonucleotide probes designed in this study were synthesized by Shanghai Sangon Biological Engineering Technology and Services (Shanghai, China), and their sequences are listed in Table S1 in Supporting information. The secondary structure of DNA probes was estimated by an online "mfold" program (*https://unafold.rna.albany.edu/*). Labeled-free and modified oligonucleotides were purified by PAGE and HPLC, respectively. All purchased oligonucleotide probes were dissolved in self-prepared buffer: 10 mM Tris, 1 mM EDTA and pH 8.0 (1 × TE buffer). BPMB probes were subjected to the thermal annealing treatment. The resulting probe solution was stored at 4 °C before use.

Streptavidin was purchased from Sigma (U.S.A), Klenow fragment polymerase (3′-5′exo-) (KFP), 10 × NE Buffer 2, mixture of deoxyribonucleotides (dNTPs) and low molecular weight ladder were purchased from New England Biolabs (Beijing, China). SYBR Green I and 6 × gel loading buffer were obtained from Dingguo Changsheng Biotechnology (Beijing, China). Human breast cancer cell line (MCF-7 cells), cervical cancer cells (HeLa cells) and human hepatocyte cells (L02 cells) were obtained from Cell Resource Center of Shanghai Institute for Biological Sciences (Chinese Academy of Sciences, Shanghai, China). Lipofectamine 2000 (Lipo2000) transfection reagent and Opti-MEM reduced serum medium (no Phenol Red) were obtained from Thermo Fisher (Waltham, USA). RIPA buffer and Phenylmethanesulfonyl fluoride (PMSF) were obtained from Beijing Dingguo Biotechnology Co., Beijing, China. BCA Protein Assay kit was acquired from Takara (Dalian, China). Other chemical reagents were of analytical grade and solutions were prepared with ultrapure water (18.25 MΩ·cm).

2D fluorescence counts of miRNA in living cells via GDPH-based imaging

All cells were cultured in DMEM medium (GIBCO, Paisley, UK) supplemented with 10% fetal bovine serum (FBS), 100 U/mL penicillin and 100 μg/mL streptomycin. Cells were kept at 37 °C with a humidified atmosphere of 5% CO_2. Additional species, insulin (0.2 U/mL), was added to the medium for culturing MCF-7. Cells were seeded on 22-mm cover glass in 12-well plastic-bottom plate and further cultured for 24 h. Then, the cells were starved by culturing in 1 mL of Opti-MEM medium (serum free) for 2 h before use.

To image target miRNA by GDPH-based system, two different solutions were prepared in advance. ***Solution A*** (150 μL): 6 μL of BPMB-21-qCy3 (10 μM), 2 μL of streptavidin (10 μM), 6 μL of dNTPs and 30 μL of 10 × NE Buffer 2 were added into 106 μL of Opti-MEM, followed by mixing and incubating at room temperature for 30 min. ***Solution B*** (150 μL): 5 μL of Lipo2000 and 3 μL of Klenow fragment (3′-5′exo-) polymerase were added into 142 μL of Opti-MEM and mixed well. Afterwards, the transfection mixture (300 μL) (called ***GDPH imaging solution***) was formed by mixing Solutions A and B and keeping at room temperature for 20 min. The cells were washed by PBS and incubated with the transfection mixture (300 μL) at 37 °C for 1 h. Subsequently, the cells were washed three times with PBS, and the cell nuclei were stained with 10 μg/mL Hoechst for 15 min, followed by the confocal fluorescence imaging on a Leica SP8 laser scanning confocal microscope.

For flow cytometry analysis, the cells were treated according to the procedure described above. However, after incubating with GDPH imaging solution for 1 h, the cells were washed with PBS, followed by detaching with 200 μL of 0.25% Trypsin without EDTA (Beijing Dingguo Biotechnology Co.) After collecting the cells by centrifugating at 1000 rpm/min, PBS (1 mL) was added and the resulting solution was subjected to flow cytometry analysis.

Tracing artificial target v-DT in living cells

The experimental procedure for tracing arbitrary target was divided into two steps. **Step 1**, an artificially-synthesized FAM-labeled DNA target (v-DT) hybridized with AS1411 was internalized into the HeLa cell by receptor-mediated endocytosis pathway. Specifically, equal amount (2 μL, 10 μM) of v-DT and AS1411 were add to 21 μL of PBS and mixed well. After 1-h incubation at room temperature, the mixture was diluted with DMEM to 500 μL, followed by incubating with HeLa cells for another 1 h. **Step 2**, GDPH-based imaging of v-DT internalized in the cells was conducted according to the procedure described in the section of "2D Fluorescence counts of miRNA in living cells via GDPH-based imaging", but BPMB-v-DT-qCy3 probe was used instead of BPMB-21-qCy3.

Simultaneous fluorescence imaging of different intracellular miRNAs

The imaging procedure was the same as the description in the section of "2D Fluorescence counts of miRNA in living cells via GDPH-based imaging", but both BPMB-21-qCy3 and BPMB-125b-qCy5 were used to report miR-21 and miR-125b, respectively.

Prediction of cell proliferation by counting GDPH fluorescent spots from 3D imaging

Cells were cultured as described in the section of "2D Fluorescence counts of miRNA in living cells via GDPH-based imaging"

and seeded in 6-well plastic-bottom plate, followed by culturing for 24 h. Then, the cells were starved by incubating in 1 mL of Opti-MEM medium (serum free) for 2 h before use.

For modulating the expression of miR-21 in live cells, e-miR-21 and Inhibitor were separately transfected into HeLa cells with Lipo2000, while PBS was set as control. The transfection process was described as follows. Two different solutions were prepared in advance. **solution A** (400 μL): 4 μL of e-miR-21 (20 μM), Inhibitor (20 μM) or PBS was added into 396 μL of Opti-MEM, followed by mixing and incubating at room temperature for 30 min. **Solution B** (400 μL): 6 μL of Lipo2000 was added into 394 μL of Opti-MEM and mixed well. Afterwards, the transfection mixture (800 μL) was obtained by mixing Solution A with Solution B and incubating at room temperature for 20 min. Then, HeLa cells were incubated in transfection mixture for 1 h. After washing with PBS, the cells were cultured in DMEM medium for another given time periods (e.g., 24 and 48 h).

For visualizing the expression level of miR-21 in live cells treated, GDPH-based 3D imaging was performed according to the procedures described in the section of "2D Fluorescence counts of miRNA in living cells via GDPH-based imaging".

For exploring the expression of miR-21 in HeLa cells by qPCR, the RNAs were extracted from the cells using Trizol Reagent Kit (Invitrogen) according to the instructions and then kept at −80 °C before use. The qPCR was conducted using the PrimeScriptTM RT reagent Kit (TaKaRa) according to manufacturer's protocol. U6 in each group of cells was selected as the endogenous control.

For western blotting analysis, HeLa cells were lysed in RIPA buffer supplemented with Phenylmethanesulfonyl fluoride (PMSF) at the ratio of 100:1. The total proteins were quantified by BCA Protein Assay kit. Equal proteins in each sample were separated by 10% SDS-PAGE and then the electrophoretic blotting was conducted to transfer the proteins to nitrocellulose membranes (NC membranes). After sealing the membranes by nonfat milk powder for 2 h at room temperature, the NC membrane was incubated with primary antibody against PDCD4 (Rabbit mAb #9535, Cell Signaling Technology) at the concentration of 1/1000 diluted in TBST [Tris-buffered saline with 0.1% (v/v) Tween-200, 5% (w/v) BSA]. Afterwards, the membrane was incubated with the corresponding HRP-conjugated secondary antibodies (HRP-linked Anti-rabbit IgG #7074, Cell Signaling Technology) (1:1000) in TBST. The immunoreactive bands were visualized by an enhanced chemiluminescence (ECL) system (Thermo Fisher, Waltham, USA), and the images were scanned by ChemiDoc XRS Imaging system (Bio-RAD, U.S.A.). The relative protein expression was measured by densitometric analysis using the Image Lab software (Bio-Rad). GAPDH (glyceraldehyde-3-phosphate dehydrogenase) was used as endogenous control.

For cell proliferation analysis, the cells were separately transfected with e-miR-21, Inhibitor and PBS, followed by culturing for 0 h, 24 h or 48 h. Afterwards the cell proliferation was evaluated by Cell Counting Kit-8 (CCK8) assay according to the instructions (Beijing Dingguo Biotechnology Co., Beijing, China).

Evaluation of tumor development by 3D counting of GDPH fluorescent spots

For modulating the expression of miR-21 in live cells, e-miR-21 and Inhibitor were separately transfected into HeLa cells as described in the section of "Prediction of cell proliferation by counting GDPH fluorescent spots from 3D imaging". The miR-21 imaging and cell viability assay were performed as described in the section of "Prediction of cell proliferation by counting GDPH fluorescent spots from 3D imaging". Female BALB/c nude mice (4–6 weeks old) were subcutaneously injected with 1×10^7 cells. After 39 days, the tumors were harvested, and the average size was measured from four independent experiments according to the formula = tumor length × (tumor width)^2/2. The animal experiment was approved by the Institutional Animal Care and Use Committee (IACUC) of Fuzhou University (approval number: SYXK-2019-0007).

Ethics statement

All experiments involving animals were conducted according to the ethical policies and procedures approved by the ethics committee of the Institutional Animal Care and Use Committee (IACUC) of Fuzhou University (approval number: SYXK-2019-0007).

Results and discussion

Working principle of catalytic assembly of GDPH for cell viability assay

The miR-21 has been discovered as only one miRNA with an overexpressed level in eleven solid cancers so far [24]. Moreover, the previously-reported molecular biology techniques have identified that miR-21 severs as an active promoter capable of down-regulating the programmed cell death 4 (PDCD4) protein and thereby exerts significant effects on the cell proliferation [24,25]. The aberrant expression levels of miR-21 are associated with early cancer diagnosis and therapy response [26]. Thus, in the current study, miR-21 was used model molecule to evaluate the cell viability by quantifying miRNA expression, while HeLa cervical carcinoma cells were used as tumor cell model. All DNA probes and miRNAs, including target miR-21 and nontarget species, are described in Table S1.

As shown in Scheme 1A, besides the schematic illustration of down-regulating programmed cell death protein, we schematically depict an intracellular *in situ* assembly of DNA-protein hybrid GDPH from A-BPMBs upon initiation of miR-21 though ^{c}SDA process in the presence of polymerase, enabling the recycle of intracellular target species and achieving the continuous growth effect. The molecular structure of A-BPMB is shown in Scheme S1. A-BPMB contains three biotinylated palindromic molecule beacons (BPMBs) with an identical base sequence that are glued together by a streptavidin. Each MB is designed as a multifunctional probe capable of serving as recognition element, polymerization primer and template. The catalytic assembly of GDPH by ^{c}SDA process is shown in Scheme 1B, and more details are presented in Scheme S2A. The hairpin-structure of BPMB is opened by miR-21 (red) after being transfected into target cells, exposing its palindromic fragment (brown). The intermolecular hybridization between opened palindromic ends preferentially occurs (step i) due to the spatial orientation-based superiority (avoiding the conformationally-constrained bent structure required for the intramolecular interaction within A-BPMB). Then, the hybridized palindromic ends serve as the primers to perform the polymerization reaction with the help of polymerase by using each other as the templates (step ii), leading to the displacement of hybridized target molecules. Subsequently, the released target miRNAs search their nearest surroundings for the next binding sites and initiate the next round reactions (step iii), resulting in net-like cross-linked structure (step iv and step v, as well as GDPH) that causes fluorescence amplification effect. Structurally, A-BPMB building blocks are assembled into two dimensional fluorescent bioarray consisting of BPMB and streptavidin. The assembled products are called grid-patterned DNA-protein hybrids (GDPHs), which look very much like fluorescent spot flares with a very high level of brightness scattered within the intracellular space. The basic structural unit of GDPH is a three-arm junction, where the central con-

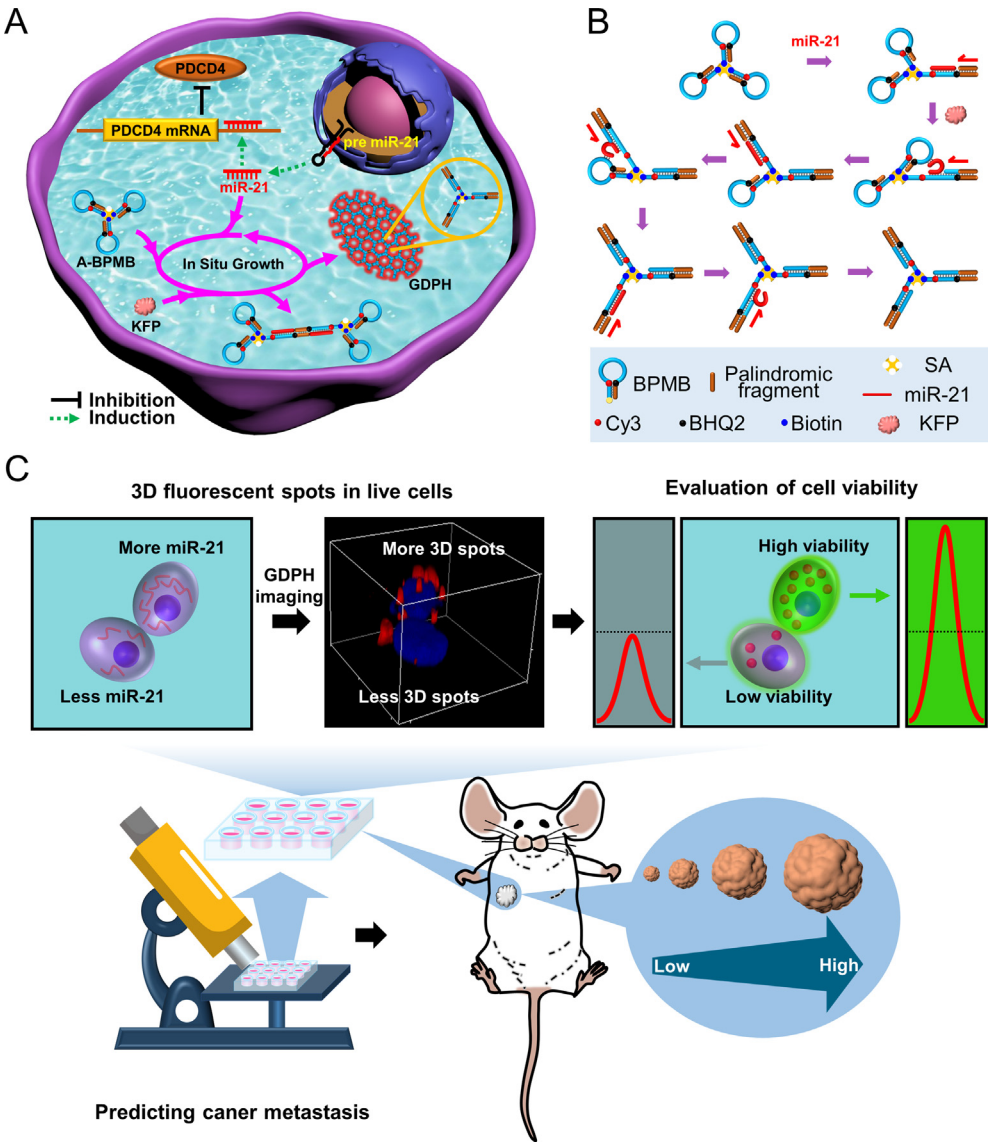

Scheme 1. The molecular mechanism for screening cell viability by fluorescently counting intracellular miRNAs via using GDPH-based system. (**A**) Schematic illustration of intracellular miR-21-induced *in situ* growth of grid-patterned DNA-protein hybrid (GDPH) and miRNA-mediated regulatory pathway in cell proliferation by targeting programmed cell death 4 (PDCD4) gene. (**B**) The cross-linking strand displacement amplification (^{c}SDA) responsible for the enzymatic assembly process of GDPH. (**C**) Screening the cell viability by counting intracellular 3D fluorescent spots for evaluating cancer metastasis.

nector is streptavidin and each arm is the double-stranded (ds) DNA, and thus GDPH exhibits hardly the intracellular mobility. As a result, its position and number are determined by the triggering molecules, intracellular miR-21. By counting the fluorescent GDPH spots visualized via confocal fluorescence microscopic imaging in three-dimensional models (Scheme 1C), miR-21 expression level is sensitively estimated with a high spatial resolution. Since miR-21 plays a key role in the PDCD4-inhibited pathway in cell proliferation by targeting related-mRNA in mammalian cells [24,25], utilizing the newly-developed GDPH-based 3D-IFC assay to quantify miR-21, the viability of tumor cells can be evaluated and the tumor recurrence and metastasis mediated by CTCs can be predicted.

Characterization of GDPH assemblies and verification of fluorescence response in vitro

Since non-denaturing gel electrophoresis is a reliable and efficient method for characterizing DNA structures [27], GDPH assembled from A-BPMB is first characterized by native-polyacrylamide gel electrophoresis (nPAGE). As shown in Fig. S1A, BPMB with only 46 bases leads to a fast-moving lowermost band in lane 1. Upon addition of streptavidin connector, a new major band with high molecular weight appears in lane 2, indicating the formation of A-BPMB. In addition to this, there is a wide faint band that should correspond to the assembled byproducts at the low ratio of BPMB-to-streptavidin. Even so, the final assemblies (Fig. S1E) and signaling capability (Fig. S4) are desirable. In lane 3, A-BPMB band become weak and new band with the lower gel mobility is detected, demonstrating the hybridization of target miR-21 to A-BPMB. Excitingly, the substantial difference between lane 4 and lane 5 offers the convincing evidence that target miR-21 does activate the assembly of GDPH with a highly-cross-linked structure from A-BPMBs. Even if much lower target concentration (100 nM) than BPMB (300 nM) is involved, no detectable residual band of A-BPMB demonstrates that target miRNA is recycled to repeatedly perform ^{c}SDA reaction, leading the exhaustion of building blocks. Although lane 4 seems unusual compared with lane 2

that also has no target molecules, the appearance of major narrow band with a reduction of electrophoretic mobility should be attributed to the interaction between A-BPMB and Klenow fragment (3′ → 5′ exo-) polymerase (KFP) according to literature report [28] rather than GDPH inadvertently generated because GDPH has the larger molecular weight. The assembly of GDPH upon miR-21 was also confirmed by fluorescence spectral measurement. As shown in Fig. S1B, there is no detectable difference in the fluorescence intensity between sample-1, sample-2 and sample-3. Only slight fluorescence increase is observed in sample 4 (blank) due to the interaction of A-BPMB with KFP, while a significantly stronger fluorescence signal is detected in sample-5 in the presence of miR-21D, demonstrating the fully-opened BPMB probes after the formation of GDPH via ^{C}SDA reaction.

To directly visualize GDPH nanoarray, we performed the characterization by atomic force microscopy (AFM) because this technique is considered to be a powerful tool for exploring the microscopic structure of DNA assemblies, including two-dimensional DNA molecular arrays [29]. As shown in Fig. S1D, the scattered bright dots with the average height of 2.33 nm are the streptavidin connectors, while BPMB arms are too small to be resolved by AFM. In contrast, Fig. S1E shows the densely-arranged grid-patterned bioarray. In the corresponding cross-section view, besides the sharp peaks of streptavidin connectors, the shoulder peaks are observed with the average height of 1.69 nm that is close to the theoretical width of double-stranded DNA fragments [30], confirming the formation of net-like cross-linked BPMBs.

In vitro miRNA detection by cross-linking strand displacement amplification (^{C}SDA)

As the central connector of structural unit of GDPH, very high or very low concentration of streptavidin (SA) disables the formation of cross-linked structure of assemblies. Thus, the dependence of GDPH assembly on the ratio of SA-to-BPMB was explored by nPAGE analysis. As shown in Fig. S2 (panel A and panel B), in the absence of SA (sample-a, 12:0), only short linear DNA products (LDP) are obtained because of the strand displacement amplification (termed ^{L}SDA), and the corresponding schematic diagram is shown in Scheme S2B. Moreover, the residual BPMB band can be detected (lane a). When gradually increasing the SA concentration to 12:3 (sample-b) and 12:4 (sample-c), a new band appears at the entrance of gel wells and the amount of LDP products decreases until disappears (sample-c), implying the generation of grid-patterned DNA-protein hybrid (GDPH) assemblies. Moreover, the residual BPMB band also completely disappears even at the same concentration of target species as sample-a, confirming the higher SDA-based signal amplification efficiency. However, if further increasing the streptavidin content, for example, sample-d (12:6) and sample-e (12:12), the assembly efficiency is compromised and even some faint smearing bands appear (lane e). The structure of main reactants at various SA-to-BPMB ratios is described in Fig. S2B. The 12:4 ratio offered the highest assembly efficiency. Thus, the optimal ratio of 12:4 was used in the subsequent experiments. Moreover, the reaction time for GDPH assembly *in vitro* was optimized by fluorescence measurement. As shown in Fig. S3, the optimal incubation time is found to be 1 h, because the longer incubation time induces the increase in background fluorescence and compromises the signal.

The capability of GDPH-based system to quantify miRNA *in vitro* was evaluated by measuring fluorescence intensity upon addition of miR-21 at different concentrations. As shown in Fig. S4A, a monotonic increase in emission intensity with increasing target concentration from 0 to 200 nM. An excellent linearity between the fluorescence signal and target concentration ranging from 0 to 50 nM is achieved (Fig. S4B), and the limit of detection (LOD) is found to be 10 pM that is capable of inducing a detectable signal higher than the background fluoresce corresponding to the blank sample. As shown in Table S2, the assay capability of GDPH-based system is 10 to 100 times higher than literature methods. Moreover, these methods are unsuitable for the *in situ* imaging of intracellular miRNAs and/or inorganic nanomaterial amplifiers are required.

The detection specificity towards target miR-21 was studied by detecting mutant counterpart species and several nontarget miRNAs coexisting within HeLa cells [31]. The sequences of mutant targets, MT1, MT2 and MT3, are shown in Table S1. As shown in Fig. S5A, the signal induced by mutant targets is less than 50% (49.8% for MT1, 26.6% for MT2 and 20.7% for MT3) if defining the fluorescence signal of miR-21D as 100%. Moreover, much lower fluorescence signal appears upon nontarget miRNAs (Fig. S5B). Specifically, the signal induced by miR-200cD, Let-7aD, Let-7cD and Let-7fD is only 2.7%, 4.5%, 6.7% and 2.9%, respectively. Thus, the quantitatively counting of miR-21 within HeLa cells is not interfered.

Time-dependent assembly of countable fluorescent GDPH spots within cells and potential application in evaluating the expression level of miRNAs

After demonstrating the desirable performance of GDPH-based system for miRNA detection *in vitro*, we explored the feasibility of *in situ* growth of GDPH within living cells and evaluated its potential application in estimating the expression of miRNAs. Considering the high efficiency of lipid-based transfection agents for promoting the cellular internalization of drug-incorporated formulations and signaling DNA probes [32], we herein used a commercial lipofectamine 2000 Reagent (Lipo2000) to transport A-BPMB into HeLa cells. The subcellular localization of GDPH assembled was explored by colocalization analysis. For this purpose, BPMB was labelled with Cy3 (red) and BHQ2 at the two ends of hairpin structure, while lysosomes were stained by Lyso Tracker (green). The growth of GDPH was monitored by cell imaging at several time points post-incubation in transfection mixture. As shown in Fig. S6, no obvious red fluorescence is detected at the initial stages (e.g., 15 min), indicating that almost no GDPH was assembled. Subsequently, the red fluorescent spots (FSs) appear and the number gradually increases. At the incubation time of 60 min, the separation of red fluorescent spots (FSs) from green clusters (indicated by white arrows) can be observed, demonstrating that A-BPMBs escaped from lysosomes, entered cytoplasm and assembled into GDPH upon initiation of miR-21. Moreover, the size of red spots increases, and they tend to aggregate (e.g., 240 min), demonstrating the gradual growth of GDPH. To accurately count the fluorescent spots for estimating the expression level of miRNAs, the incubation time of 60 min was chosen for the intracellular assembly of GDPH to obtain the well dispersed fluorescent flares.

To demonstrate the feasibility of as-proposed GDPH counting-based strategy for evaluating the expression level of miRNAs, a well-known method, which is based on the fluorescent spot counting in the two dimensional space within cells [13] (called 2D fluorescence counts herein), was used to analyze HeLa cells. For comparison, human breast cancer cell lines (MCF-7 cells) and normal human hepatocyte cell lines (L02 cells) were employed as the positive control and negative control, respectively, since miR-21 was reported to be overexpressed in the former but not in the latter [33]. As shown in Fig. 1A, as expected, the average number of fluorescent GDPH spots within MCF-7, HeLa and L02 cells is 6.0, 3.2 and 0, respectively. Namely, the miR-21 expression level decreases in the trend: MCF-7 > HeLa > L02 cells, which is in good agreement with the experimental results from flow cytometric analysis (Fig. 1B), showing the potential application in screening the expression profile of intracellular miRNAs.

Stability of 2D GDPH nanostructure in live cells

While versatile DNA structural nanotechnology makes DNA nanostructures, including two-dimensional (2D) arrays, useful for various biological applications, the susceptibility of common DNA assemblies to attack by nucleases present in complicated physiological media become the major roadblock to clinical translation [34]. Thus, the degradation resistance of GDPH assembly was explored in nuclease solution in tube format and within living cells. DNase I was used as the nuclease model because of its high capability to nonspecifically cleave ssDNA and dsDNA [12,35], and the residual GDPH digested by DNase I (2 U/mL) was evaluated by gel electrophoresis analysis. As shown in Fig. S7, GDPH can exist in DNase I for at least 4 h even if exposed to 20 times higher concentration of DNase I than literature value [36], while the corresponding linear DNA counterpart products are completely digested within less than 1 h, demonstrating the substantially enhanced nuclease-degradation resistance of GDPH.

Taking into account that DNA assemblies are more easily degraded in complicated intracellular environment where there are a wide variety of biological progresses besides biomolecules [37], the intracellular stability of GDPH was also evaluated, where linear DNA counterpart product (LDP) was used as control. As shown in Fig. S8, no substantial decrease in the fluorescence intensity is detected for intracellularly assembled GDPH after 6-h incubation. In sharp contrast, the signal of LDP almost disappears at 6-h incubation under identical conditions despite that LDP-based system possesses a desirable assay performance *in vitro* (Fig. S9). These experimental results demonstrate that 2D GDPH nanostructure exhibits substantially enhanced stability inside live cells so that researchers are allowed to have time to collect the sufficient information of intracellular miRNAs [33]. Moreover, GDPH probes show good biocompartibility and do not influence the cell viability even if the higher concentration of probes are transfected into living cells as described in Fig. S10.

Suitability of GDPH counting for in situ imaging of intracellular biomolecules and superiority of 3D counting over 2D counting

The intracellular mobility of internalized materials, as well as exocytosis [38] and cell permeability that may be disturbed by external factors (e.g., transfection agents) [39], can influence their location and distribution within cells. Thus, it is necessary to study the apparent intracellular mobility (AIM) of 2D GDPH. For this purpose, MCF-7 cells were fixed with paraformaldehyde and permeabilized in order to allow large biomolecules readily diffuse through the cell membrane according to literature methods [33]. As shown in Fig. S11, very strong red fluorescence is detected for GDPH-based system (panel a), demonstrating that GDPH assemblies can firmly reside inside cells even if undergoing washing treatment. Even in the absence of polymerase that is required for the cross-linking assembly process, the detectable fluorescence is still observed (panel b), which should be attributed to the steric hindrance originating from the branched structure of A-BPMB upon miR-21. In contrast, no fluorescence signal is detected for LDP-based system (panel c) even if it emits a strong fluorescence signal in normal solution (Fig. S9). This is because the linear products easily diffuse out of cells during washing treatment. Similarly, there is no fluorescence signal for panel d.

Subsequently, the suitability of GDPH-based system for intracellular *in situ* imaging of miRNAs were examined by performing the colocalization of its Cy3 fluorescence signal (red) with a 'visible' DNA target molecule (v-DT) that was labelled with FAM fluorophore (green) and pre-hybridized with aptamer AS1411. The experimental procedure is outlined in Fig. 2A. AS1411 was reported to specifically recognize the nucleolin expressed in various cancer cells, such as HeLa [40], and thus v-DT/AS1411 hybrid can be internalized into HeLa cells by receptor-mediated endocytosis pathway. As shown in Fig. 2B, after exposure of v-DT/AS1411-internalized cells to GDPH imaging solution, both red and green fluorescence signals are observed, indicating the internalization of v-DT and formation of GDPH. Moreover, besides the high degree of overlap with a MCC value of 0.949, the red fluorescence is highly associated with green fluorescence (PRC = 0.436) [41]. For the magnified images (Regions 1f, 2f, 3f and 4f), the overlap of red fluorescence with green fluorescence can be observed more clearly regardless of whether the green fluorescence signal is strong (e.g., Regions 1d and 2d) or weak (e.g., Regions 3d and 4d).

Because 3D imaging can theoretically collect as many optical sections as researchers want and offer sufficient information on intracellular biomolecules [42], the comparative study of assay performance of 3D- and 2D-based imaging techniques were conducted. To obtain 2D fluorescence images on the different optical sections of model cells, the confocal fluorescence imaging of HeLa

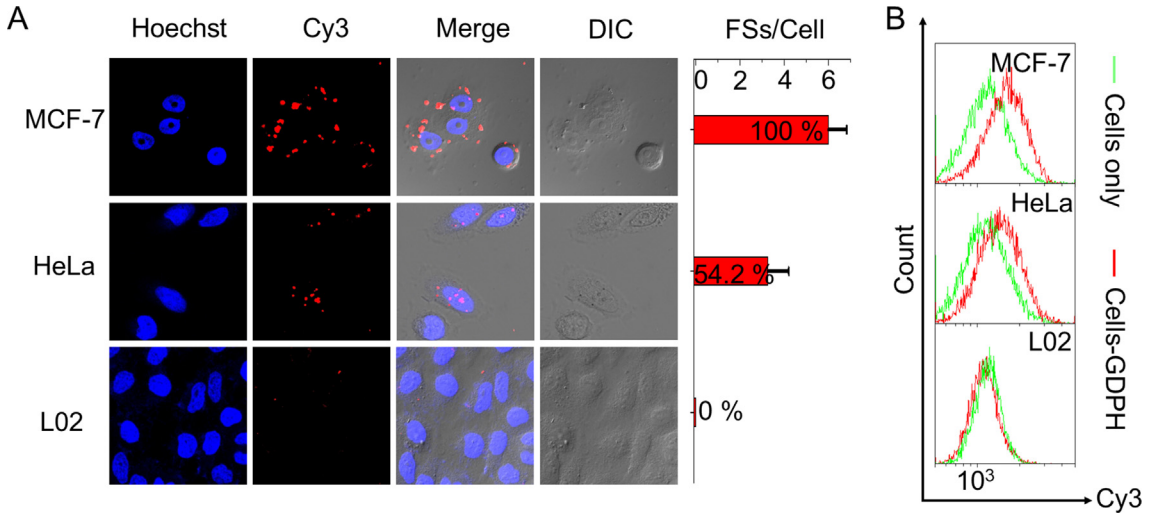

Fig. 1. 2D imaging of miR-21 in live cells by GDPH-based system. (**A**) Confocal fluorescence imaging of miR-21 in MCF-7 cells (upper panel), HeLa cells (middle panel) and L02 cells (lower panel). The red fluorescence represents Cy3-labelled GDPH spots, and cell nuclei are stained with Hoechst. The average number of fluorescent GDPH spots per cell (FSs/cell) is shown in the right panel. (**B**) Flow cytometric analysis of the corresponding samples, where cells only were used as control (green line).

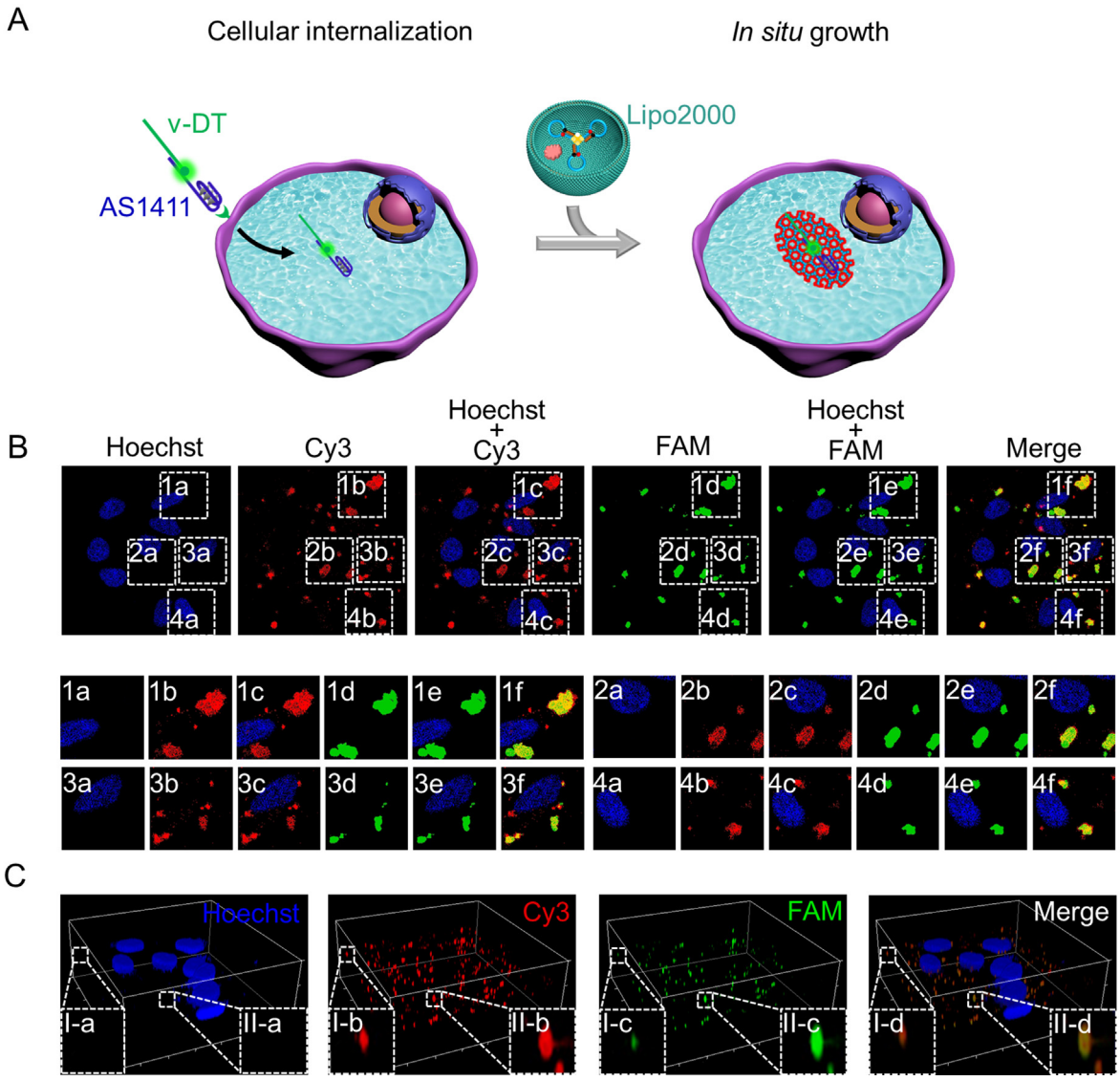

Fig. 2. ***In situ*** **growth of GDPH architecture triggered by artificial 'visible' target species in live cells.** (**A**) Schematic illustration of aptamer-mediated internalization of FAM-labelled v-DT target into HeLa cells, followed by the assembly of GDPH architecture from A-BPMBs transfected by Lipo2000. (**B**) Colocalization of FAM-attached v-DT and Cy3-modified A-BPMB building blocks within HeLa cells by 2D fluorescence imaging to demonstrate the *in situ* growth of GDPH architecture. Pearson's correlation coefficient (PRC), 0.436; Manders' colocalization coefficients (MCC), 0.949. The regions boxed with white lines are enlarged in the lower panel to observe the relative location of triggering v-DT and GDPH assemblies. (**C**) 3D fluorescence images of HeLa cells undergone the same treatment as (B), where the fluorescent spots boxed by white lines are enlarged to observe the assemblies more clearly. PRC is 0.403, while MCC is 0.997. Green and red fluorescence spots denote v-DT and GDPH, respectively. Blue fluorescence represents cell nuclei stained with Hoechst.

cells was performed while gradually moving the microscope stage from the cell top down to dish bottom by preset distances. The resulting four 2D fluorescence images at different Z-depths are presented in Fig. S12B, which are broken down into locally-enlarged fluorescence images in Fig. S12C to extract more detailed information. One can notice that 18-μm-depth 2D image loses the information from other optical sections, such as fluorescent spots indicated by white, yellow, and green arrows at the Z-depths of 15 μm, 21 μm and 23 μm, respectively, which is consistent with the theoretical mechanism for Z-series [42]. Unlike the 2D image, the corresponding 3D fluorescence image contains almost all the detectable information of miRNAs within cells as shown in Fig. S12A, and the discrete red spots is countable, confirming the superiority of 3D fluorescence imaging over 2D imaging [42].

Along this line, the colocalization assay of triggering molecules and assembled products within HeLa cells treated with the same procedure described in Fig. 2B was performed in 3D projection, and the results are shown in Fig. 2C. Clearly, different red (or green) fluorescent spots are spatially well separated from each other, and signal amplification effect is achieved (e.g., very weak green fluorescence in region I-c induces a strong red signal in region I-b), enabling the quantification detection of triggering molecules more accurately by counting the red spot number. Moreover, the capability of 3D imaging to screen the relationship between v-DT triggers and GDPH assemblies is not compromised (i.e., comparable PRC value and higher MCC value). Interestingly, because AS1411 specifically binds the nucleolin, it can be expected that intracellular proteins of interest is able to be *in situ* screened

by GDPH-based system with the help of targeting ligands, such as DNA aptamers and other bioactive molecules [43].

Capability of GDPH-based 3D-IFC technique to quantify miRNA in individual cells

Since the fluorescent GDPH spots is countable in 3D space, 3D counting of intracellular fluorescent spots (3D-IFC) is expected to become an accurate method to estimate the expression of miRNAs, establishing the technical basis for imaging biomarkers in individual cells. The utility of GDPH-based 3D-IFC technique was examined by analyzing miR-21 content in MCF-7 and HeLa cells. The 3D images of MCF-7 and HeLa cells are shown in the upper panels of Fig. S13A and S13B, respectively, while the number of red GDPH spots per cell is presented in the lower panel (fluorescent spots are thought to belong to the nearest cells). The density of red spots in the 3D image of MCF-7 cells is much higher than HeLa cells. It is also interesting to notice that, for the same type of cells, the number of red spots within different numbered cells is different from each other, reflecting the different expression level of miR-21 in individual cells (i.e., tumor cell heterogeneity), which agrees well with literature reports [44]. The 3D imaging of three different kinds of cells (L02 cells used as negative control) was performed in the same way and the results of statistical analysis of FSs/Cell are shown in Fig. S14. The average FS number is 13.6, 5.0, and 0 FSs/Cell for MCF-7, HeLa and L02 cells, respectively, indicating 36.9% for HeLa and 0% for L02 if defining the expression level of miR-21 in MCF-7 cells as 100%. The FS number detected from positive MCF-7 and HeLa cells by 3D-IFC-based assay is much higher than the corresponding number offered in Fig. 1, implying that 2D imaging-based FS counting does lose about half of fluorescent flares. As a gold standard to evaluate the content of miRNAs with high sensitivity [45], the quantitative PCR (qPCR) was conducted for determining the expression of miR-21 in the three cell lines, and the results are shown in Fig. S15 and Table S3. The content of miR-21 in HeLa cells is 0.375 by normalizing the miR-21 expression in MCF-7 cells to equal 1. As expected, the 3D-IFC technique offers the more accurate test results than the conventional 2D-based fluorescence counting (Fig. 1A), providing researchers a good opportunity for single-cell analysis often required by disease diagnosis and prevention.

Universality of GDPH-based 3D-IFC for quantitatively evaluating the expression of intracellular miRNAs

A diversity of miRNAs was reported to mediate various pathways involved in complex gene regulatory networks [46]. To study the universal applicability of GDPH-based 3F-IFC assay for miRNA quantification in living cells, another miRNA, miRNA-125b (miR-125b), was detected in HeLa cells because it is reported to be a prognostic biomarker capable of regulating multiple target genes [47] and is moderately expressed in HeLa cells [31]. Probe of miR-125b (BPMB-125b-qCy5) was simply designed by substituting the original recognition site of BPMB-21-qCy3 with the complementary fragment of miR-125b (seen in Table S1). The *in vitro* tests were described in Fig. S16. The increase in the concentration of miR-125bD (synthetic DNA analogue of miR-125b) leads to a monotone increase of fluorescence signal (Fig. S16A), exhibiting a good linear relationship between the fluorescence intensity and target concentration in a range from 0 to 100 nM (Fig. S16B). Fig. S17 shows the intracellular imaging of miR-125b in HeLa cells, accompanied by the quantitative evaluation of its content by counting fluorescent spots. The Cy5-lablled GDPH intracellularly assembled from A-BPMB probes upon activation of miR-125b can be clearly detected, and the average number of fluorescent spots (FSs/Cell) are 1.6 and 1.0 for 3D- and 2D-based counting, respectively, implying the feasibility of GDPH-based 3D-IFC assay for intracellular quantification of miR-125b and exhibiting the superiority overt 2D fluorescence counts because some fluorescent spots are lost for 2D-based counts.

To examine the ability of GDPH-based 3D-IFC assay to simultaneously detect different miRNAs (e.g., miR-21 and miR-125b), the double-channel-based 3D fluorescence imaging was performed after treating HeLa cells with GDPH imaging solution containing BPMB-125b-qCy5 and BPMB-21-qCy3. L02 cells were used as negative control. The corresponding scheme is illustrated in Fig. 3A, while the experimental results are shown in Fig. 3B. The red and green fluorescence signals are detected for HeLa cells but not for L02 cells, verifying the assembly of different GDPH products within HeLa cells on activation of miR-21 and miR-125b. Moreover, as shown in the right panel, the expression level of two miRNAs can be quantified by separately counting the number of corresponding FSs. The contents of miR-21 (5.1 FSs/cell) and miR-125b (1.5 FSs/-cell) are consistent with the measured values of miR-21 alone in the middle panel of Fig. S14 and miR-125b alone in the upper panel of Fig. S17, respectively, evidencing that the different GDPH assembly processes upon two biomolecules proceed independently and do not interfere with each other. Fig. 3C shows the enlarged 3D images of boxed Regions a and b in Fig. 3B. The red and green fluorescent spots do completely separate from each other (confirmed by extremely low PRC value), implying that multiple targets within the same cells can be simultaneously detected by GDPH-based 3D fluorescent spot counting. If defining the expression of miR-21 as 100%, the relative expression level of miR-125 is 28.3% by 3D-IFS, which is comparable to qPCR gold standard assay (seen in Fig. S18 and Table S4), while the value of 38.1% from 2D fluorescent spot counting is obviously higher. Presumably, this is because some fluorescent spots, especially the red spots, were missed during 2D counting. The negative L02 cells (lower panel of Fig. 3B) and scrambled Mis-probe (Fig. S19) that can recognize neither miR-21 nor miR-125b have no detectable FSs, indicating that the FSs are specifically formed from target miRNA-induced self-assembly from A-BPMB probes.

Relationship between cell proliferation and fluorescence signal from GDPH-based 3D-IFC assay

Fig. 4A illustrates the 3D fluorescent prediction of tumor cell proliferation via estimating the expression of miR-21 by GDPH-based 3D-IFC assay. The increase in miR-21 expression level can downregulate the expression of PDCD4 protein and favor cell proliferation [24,25]. To confirm the relationship between cell proliferation and fluorescence signal from GDPH-based 3D-IFC assay, we recorded the fluorescence signal by calculating FSs/cell from three different groups of HeLa cells (e-miR-21-transfected cells, intact cells and Inhibitor-transfected cells) with different miR-21 contents and tested relative cell growth rate. Fig. 4B shows 3D fluorescence images. The decrease in the density of red GDPH spots follows the trend: e-miR-21-transfected cells > intact cells > Inhibitor-transfected cells. If the fluorescence signal induced by the highest content of miR-21 in exogenous e-miR-21-transfected HeLa cells is defined as 100%, the signals from intact cells and Inhibitor-transfected cells are 15.2% and 3.9%, respectively. The relative content of miR-21 estimated by 3D-IFC assay in the three groups of HeLa cells is generally consisted with the results measured by gold standard qPCR assay (seen in Fig. 4C and Table S5). Moreover, the PDCD4 protein was analyzed by western blot and cell proliferation was detected by CCK-8 kit. The corresponding results are presented in Fig. 4D and in Fig. 4E, respectively. The high level of PDCD4 is observed in Inhibitor-transfected HeLa cells, while the e-miR-21-transfected cells express a very low level of PDCD4, evidencing the negative regula-

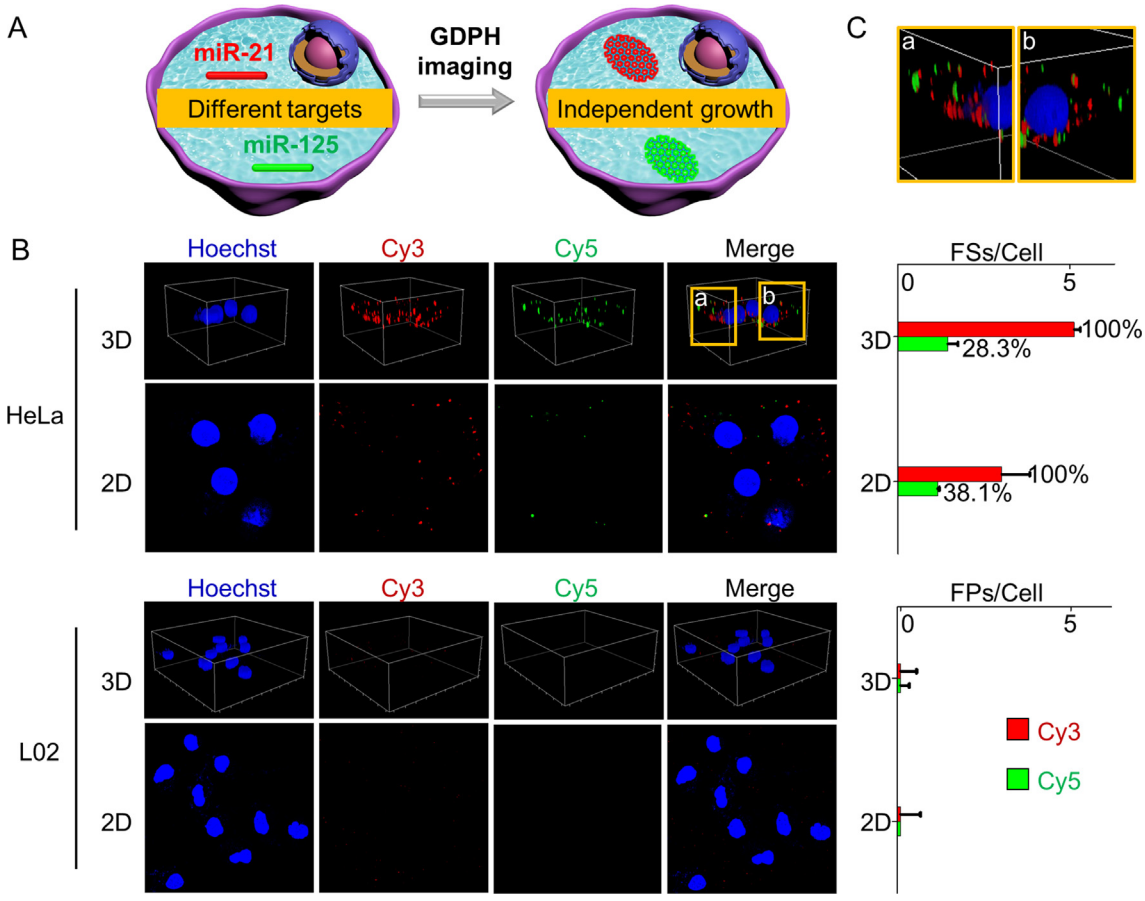

Fig. 3. Comparative study of the performance between 2D- and 3D-based fluorescence counts by GDPH-based system. (**A**) Schematic illustration of double-channel fluorescence analysis. Simultaneous fluorescence imaging of miR-21 (Cy3, red fluorescence) and miR-125b (Cy5, green fluorescence) within HeLa cells or L02 cells (**B**). The average number of fluorescent GDPH spots per cell (FSs/cell) is shown in the right panels. (**C**) The high resolution images of the two regions boxed in (B). The PRC values in Regions a and b are −0.511 and −0.551, respectively. Cell nuclei were stained with Hoechst. BPMB-21-qCy3 and BPMB-125b-qCy5 were used to recognize miR-21 and miR-125b, respectively.

tion of PDCD4 by miR-21. The relative cell growth (RCG) of e-miR-21-transfected cells, intact cells and Inhibitor-transfected cells are 227%, 168%, and 132%, respectively, 2 days post-transfection, showing that cell proliferation is closely associated with intracellular miR-21 level detected by GDPH-based 3D-IFC assay. Fig. 4F directly shows a good linear correlation between RCG and logarithm of FSs/cell, demonstrating that GDPH-based 3D-IFC assay possess the potential application in evaluating the cell proliferation by counting the number of FSs fluorescently visualized inside cells. In addition, inhibition of intracellular miR-21 causes the profound suppression of the proliferation of HeLa cells, implying that the timely targeted intervention at the cellular level is a promising therapeutic direction for the prevention of cancer metastasis.

Calcein-AM assay also confirms the consistency between cell viability and fluorescence signal offered by GDPH-based 3D-IFC assay (Fig. S20). Moreover, GDPH-based 3D-IFC assay can be employed to distinguish HeLa cells with different cell viabilities coexisting in the same solution in individual cells as shown in Fig. S21 (mixture of intact cells and miR-21-upregulated cells), Fig. S22 (intact cells alone) and Fig. S23 (miR-21-upregulated cells alone), where Calcein-AM for staining living cells and/or propidium iodide (PI) for staining dead cells were used.

Predicting tumor metastasis by GDPH-based 3D-IFC technique

Since CTCs, as tumor cells present in the peripheral blood of many cancer patients, are believed to be associated with tumor clinic prognosis and metastasis [48,49], we evaluated the potential application of GDPH-based 3D-IFC assay in predicting the cancer metastasis via using HeLa cells as model CTCs. For this purpose, two groups of female BALB/c nude mice (~20 g body weight each) were separately inoculated with two populations of HeLa cells (1×10^7 cells per mouse) that were transfected with e-miR-21 or Inhibitor, followed by measurement of tumor volume. The miR-21expression level and cell viability of the two groups of HeLa cells were estimated by GDPH-based 3D-IFC assay and CCK8-kit, respectively. Fig. 5A shows 3D fluorescence images of cells treated with GDPH-based system, while Fig. 5B describes the corresponding miR-21 expression level tested by counting the number of fluorescent GDPH spots. The cell viability is quantitatively presented in Fig. 5C. The *in vitro* scratch wound healing assay is shown in Fig. S24, offering the comparative analysis of cell migration of the two groups of HeLa cells. Representative photos of tumor-bearing mice and tumors harvested 39 days post-inoculation of cells are shown in Fig. 5D, while tumor size is seen in Fig. 5E. As expected, the e-miR-21-transfected HeLa cells have the stronger GDPH fluorescence signal, exhibit the higher cell viability and possess higher capability to cause the tumor formation than Inhibitor-transfected cells, indicating that cancer metastasis can be predicted via analyzing the miR-21-mediated aggressiveness of CTCs by GDPH-based 3D-IFC assay. Moreover, no tumor was formed in about half of the mice inoculated with Inhibitor- transfected HeLa cells, evidencing that GDPH-based 3D-IFC assay is a promising valuable tool for estimating preventive treatments against tumor metastases.

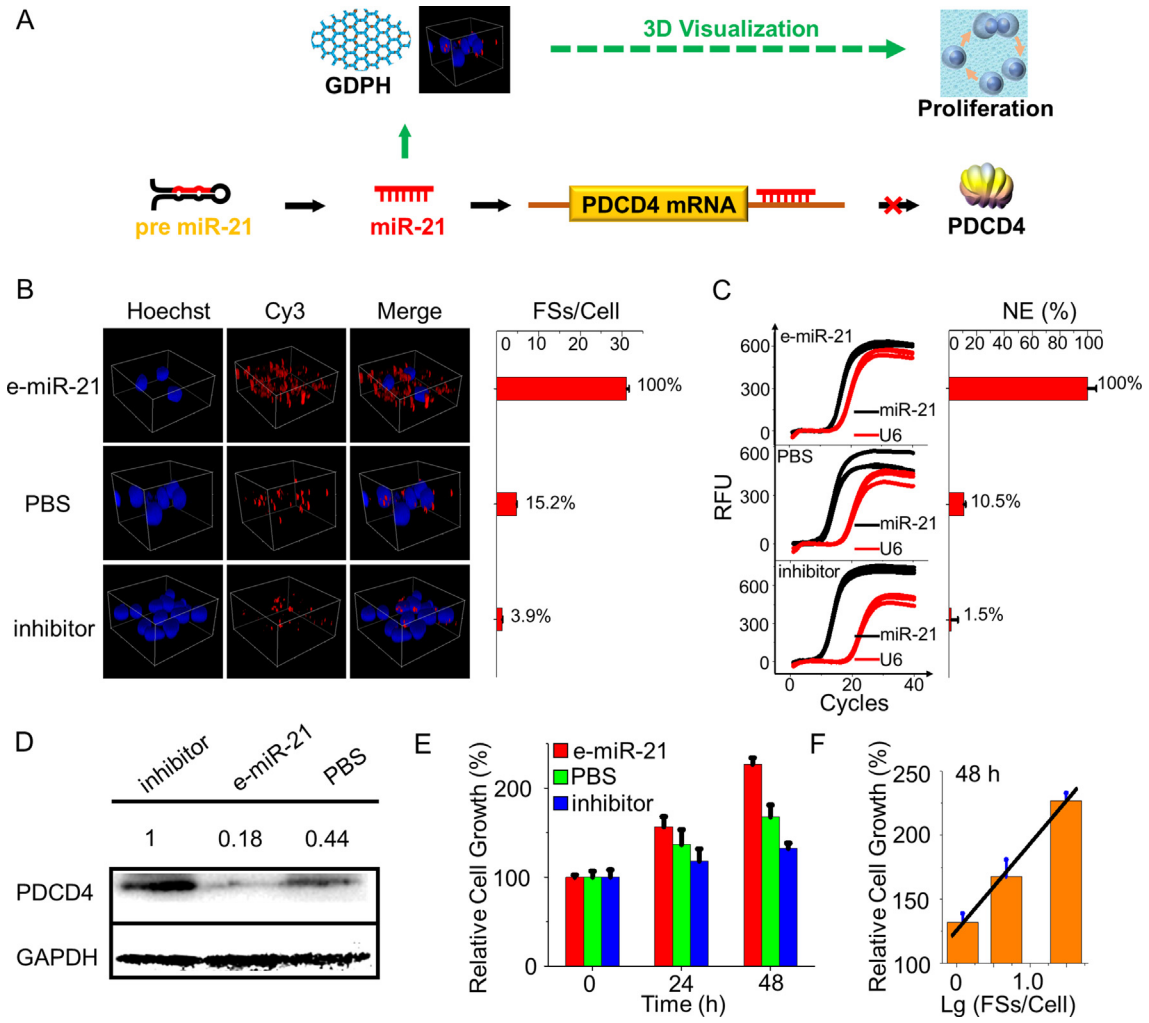

Fig. 4. Evaluating cell proliferation rate via counting miRNA by GDPH-based 3D-IFC assay. (**A**) Scheme for 3D fluorescent prediction of miRNA-mediated cell proliferation by imaging *in situ* growth of GDPH initiated by miR-21 capable of inhibiting the expression of PDCD4 protein upon targeting the corresponding mRNA. (**B**) 3D fluorescence imaging of miR-21 in HeLa cells separately transfected with exogenous miR-21 mimics (e-miR-21), Inhibitor and PBS and then cultured for 48 h. The average number of fluorescent GDPH spots per cell (FSs/cell) is shown in the right panel. The expression of miR-21 and PDCD4 protein in the three groups of HeLa cells in (B) were analyzed by qPCR (**C**) and western blot (**D**), respectively. NE: normalized expression; RFU: relative fluorescence units. (**E**) The corresponding relative cell growth (RCG) quantified by CCK8 assay. (**F**) The correlation between the relative cell growth (RCG) and logarithm of the value of FSs/Cell, which can be fitted to the following equation: RCG = 67.52 Log (FS number) + 125.03. The correlation coefficient, R^2, is 0.9974. The incubation time for cell culture was 48 h.

Conclusion

In summary, we propose a three-dimensionally (3D) counting of intracellular fluorescent spots (3D-IFC) for quantitatively estimating the expression level of miRNAs in individual cells by 3D fluorescence imaging based on the intracellular *in situ* assembly of GDPH in a stimuli-responsive fashion. The fluorescence quantification technique demonstrated in this study is important because of its several attractive advantages. (i) *In situ* imaging of intracellular target miRNAs. The assembled products show high nuclease-degradation resistance and substantially-enhanced intracellularly mobility, thus reflecting the intracellular original location and distribution; (ii) Simple and accurate fluorescence spot counts. Intracellular GDPH assemblies are discrete objects with high spatial resolution and the number is less than forty, making the counting very easily. 3D fluorescence counts can ensure the sufficient information on miRNA expression, displaying the superiority over 2D fluorescence counts; (iii) Efficient signal amplification. Target miRNA can be repeatedly recycled to trigger the GDPH assembly, leading to the restoration of initially-quenched fluorescence emission of many BPMB probes; (iv) Simple probe design. Although an efficient ^{c}SDA process is achieved, only one type of DNA probe is involved in GDPH-based system because of palindromic fragment is introduced into the end of BPMB; (v) Suitability for the *in situ* imaging of protein biomarkers by utilizing targeting ligands. Moreover, the simultaneous detection of multiple targets can be conducted within the same cell without any disturbance, while the probe is designed only thought substituting the hairpin loop with new recognition site. More significantly, GDPH probes have good biocompatibility and do not cause cell damage. Therefore, GDPH-based system is suitable for screening aggressive CTCs and predicting the metastasis formation by estimating the cell viability at the single-cell level, thus holding great potential for risk evaluation and prevention of cancer metastasis. We expect that our work on *in situ* imaging of intracellular miRNAs based on GDPH-based system provides a valuable tool for evaluating the functions of disease

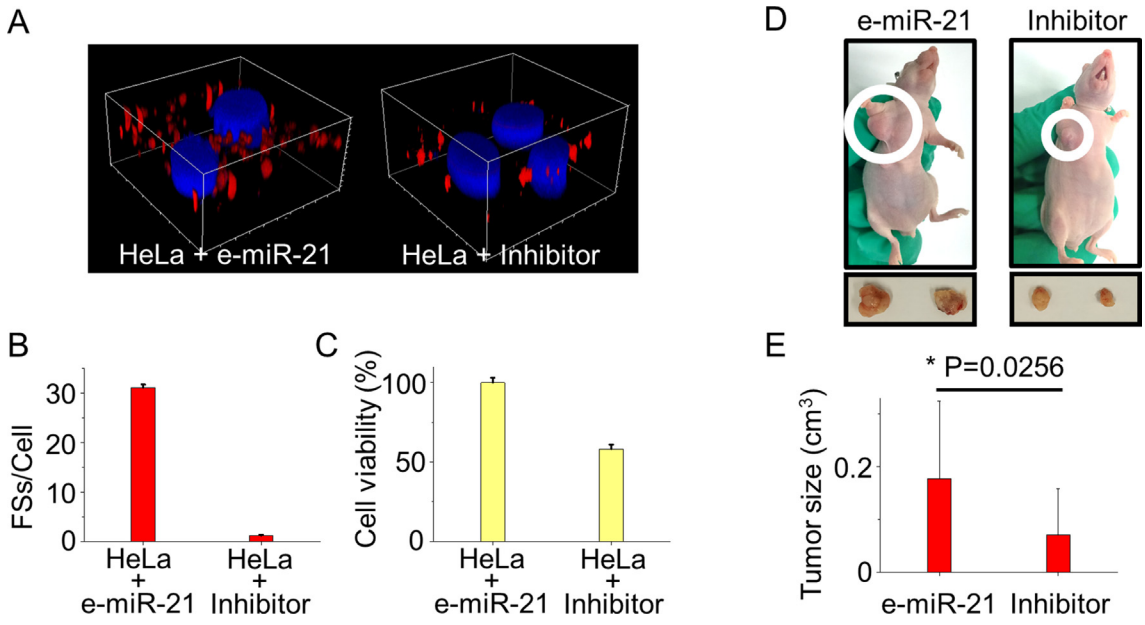

Fig. 5. GDPH-based 3D fluorescence imaging of cells for predicting cancer metastasis. (A) 3D fluorescence images of HeLa cells transfected with e-miR-21 (left) or Inhibitor (right) by GDPH-based system. **(B)** The average number of fluorescent GDPH spots per cell (FSs/cell) calculated from panel A. **(C)** The cell viability measured by CCK8 assay. (**D**) The representative pictures of tumor-bearing mice on the 39th day after subcutaneous injection of HeLa cells transfected with e-miR-21 or Inhibitor. The lower half, representative photos of tumors harvested. **(E)** The tumor size (V) estimated by the formula: V = tumor length×(tumor width)^2/2. The data were calculated from four independent experiments. The experimental procedure is described in the Section of "**Materials and methods**". The measured data are expressed as the means ± SD (n = 4). *P < 0.05, one-tailed paired *t* test.

biomarkers and in turn cellular behaviors (e.g., cell proliferation), opening profound insight into further expansion of DNA structural nanotechnology in the diagnosis and prevention of human cancers.

Compliance with Ethics Requirements

All Institutional and National Guidelines for the care and use of animals (fisheries) were followed.

The animal experiment was approved by the Institutional Animal Care and Use Committee (IACUC) of Fuzhou University (approval number: SYXK-2019-0007).

CRediT authorship contribution statement

Chang Xue: Data curation, Formal analysis, Investigation, Methodology, Software, Writing - original draft. **Huimin Niu:** Data curation, Formal analysis, Investigation, Methodology, Software. **Shuyao Hu:** Investigation. **Zhe Yang:** Data curation, Formal analysis, Methodology. **Lei Wang:** Investigation. **Zai-Sheng Wu:** Conceptualization, Funding acquisition, Project administration, Resources, Supervision, Writing - review & editing.

Declaration of Competing Interest

The authors declare that they have no known competing financial interests or personal relationships that could have appeared to influence the work reported in this paper.

Acknowledgements

This work was financially supported by National Natural Science Foundation of China (NSFC) (grant NO: 22174020 and 21775024), and Key Project of Natural Science Foundation of Fujian Province (Grant NO: 2019J02005).

Appendix A. Supplementary material

Supplementary data to this article can be found online at https://doi.org/10.1016/j.jare.2022.03.001.

References

[1] Abreu M, Cabezas-Sainz P, Alonso-Alconada L, Ferreirós A, Mondelo-Macía P, Lago-Lestón RM, et al. Circulating Tumor Cells Characterization Revealed TIMP1 as a Potential Therapeutic Target in Ovarian Cancer. Cells 2020;9 (5):1218. doi: https://doi.org/10.3390/cells9051218.
[2] Müllen K. Molecular defects in organic materials. Nat Rev Mater 2016;1:15013–4.
[3] Lu S, Wang T, Zhang G, He Q-Y. Understanding the proteome encoded by "non-coding RNAs": new insights into human genome. Sci China Life Sci 2020;63 (7):986–95.
[4] Lilley DMJ. The Ribosome Functions as a Ribozyme. ChemBioChem 2001;2 (1):31–5.
[5] Gebert LFR, MacRae IJ. Regulation of microRNA function in animals. Nat Rev Mol Cell Biol 2019;20:21–37.
[6] Bhatti I, Lee A, James V, Hall RI, Lund JN, Tufarelli C, et al. Knockdown of microRNA-21 inhibits proliferation and increases cell death by targeting programmed cell death 4 (PDCD4) in pancreatic ductal adenocarcinoma. J Gastrointest Surg 2011;15(1):199–208.
[7] Kong YW, Ferland-McCollough D, Jackson TJ, Bushell M. microRNAs in cancer management. Lancet Oncol 2012;13(6):e249–58.
[8] Cheng CJ, Bahal R, Babar IA, Pincus Z, Barrera F, Liu C, et al. MicroRNA silencing for cancer therapy targeted to the tumour microenvironment. Nature 2015;518(7537):107–10.
[9] Ling H, Fabbri M, Calin GA. MicroRNAs and other non-coding RNAs as targets for anticancer drug development. Nat Rev Drug Discov 2013;12(11):847–65.
[10] Geng J, Li W, Zhang Y, Thottappillil N, Clavadetscher J, Lilienkampf A, et al. Radical polymerization inside living cells. Nat Chem 2019;11(6):578–86.
[11] Duan R, Zuo X, Wang S, Quan X, Chen D, Chen Z, et al. Lab in a tube: ultrasensitive detection of microRNAs at the single-cell level and in breast cancer patients using quadratic isothermal amplification. J Am Chem Soc 2013;135(12):4604–7.
[12] Li C, Luo M, Wang J, Niu H, Shen Z, Wu Z-S. Rigidified DNA Triangle-Protected Molecular Beacon from Endogenous Nuclease Digestion for Monitoring microRNA Expression in Living Cells. ACS Sens 2020;5(8):2378–87.
[13] Deng R, Tang L, Tian Q, Wang Y, Lin L, Li J. Toehold-initiated rolling circle amplification for visualizing individual microRNAs in situ in single cells. Angew Chem Int Ed 2014;53(9):2389–93.

[14] Keum J-W, Bermudez H. Enhanced resistance of DNA nanostructures to enzymatic digestion. Chem Commun 2009(45):7036–8. doi: https://doi.org/10.1039/b917661f.
[15] You M, Chen Y, Zhang X, Liu H, Wang R, Wang K, et al. An autonomous and controllable light-driven DNA walking device. Angew Chem Int Ed 2012;51(10):2457–60.
[16] LaBoda C, Duschl H, Dwyer CL. DNA-enabled integrated molecular systems for computation and sensing. Acc Chem Res 2014;47(6):1816–24.
[17] Randeria PS, Seeger MA, Wang X-Q, Wilson H, Shipp D, Mirkin CA, et al. siRNA-based spherical nucleic acids reverse impaired wound healing in diabetic mice by ganglioside GM3 synthase knockdown. Proc Natl Acad Sci USA 2015;112(18):5573–8.
[18] Zhu G, Mei L, Vishwasrao HD, Jacobson O, Wang Z, Liu Y, et al. Intertwining DNA-RNA nanocapsules loaded with tumor neoantigens as synergistic nanovaccines for cancer immunotherapy. Nat Commun 2017;8(1):1482. doi: https://doi.org/10.1038/s41467-017-01386-7.
[19] Mei Q, Wei X, Su F, Liu Y, Youngbull C, Johnson R, et al. Stability of DNA origami nanoarrays in cell lysate. Nano Lett 2011;11(4):1477–82.
[20] LaBean TH, Yan H, Kopatsch J, Liu F, Winfree E, Reif JH, et al. Construction, Analysis, Ligation, and Self-Assembly of DNA Triple Crossover Complexes. J Am Chem Soc 2000;122(9):1848–60.
[21] Aldaye FA, Palmer AL, Sleiman HF. Assembling materials with DNA as the guide. Science 2008;321(5897):1795–9.
[22] Liu S, Jiang Q, Zhao X, Zhao R, Wang Y, Wang Y, et al. A DNA nanodevice-based vaccine for cancer immunotherapy. Nat Mater 2021;20(3):421–30.
[23] Zhang T, Tian T, Zhou R, Li S, Ma W, Zhang Y, et al. Design, fabrication and applications of tetrahedral DNA nanostructure-based multifunctional complexes in drug delivery and biomedical treatment. Nat Protoc 2020;15(8):2728–57.
[24] Yao Q, Xu H, Zhang Q-Q, Zhou H, Qu L-H. MicroRNA-21 promotes cell proliferation and down-regulates the expression of programmed cell death 4 (PDCD4) in HeLa cervical carcinoma cells. Biochem Biophys Res Commun 2009;388(3):539–42.
[25] Sarkar J, Gou D, Turaka P, Viktorova E, Ramchandran R, Raj JU. MicroRNA-21 plays a role in hypoxia-mediated pulmonary artery smooth muscle cell proliferation and migration. Am J Physiol: Lung Cell Mol Physiol 2010;299(6):L861–71.
[26] Tavallaie R, McCarroll J, Le Grand M, Ariotti N, Schuhmann W, Bakker E, et al. Nucleic acid hybridization on an electrically reconfigurable network of gold-coated magnetic nanoparticles enables microRNA detection in blood. Nat Nanotechnol 2018;13(11):1066–71.
[27] Kwon PS, Ren S, Kwon S-J, Kizer ME, Kuo L, Xie Mo, et al. Designer DNA architecture offers precise and multivalent spatial pattern-recognition for viral sensing and inhibition. Nat Chem 2020;12(1):26–35.
[28] Gao X, Gethers M, Han S-P, Goddard WA, Sha R, Cunningham RP, et al. The PX Motif of DNA Binds Specifically to Escherichia coli DNA Polymerase I. Biochemistry 2019;58(6):575–81.
[29] Wang D, Song J, Wang P, Pan V, Zhang Y, Cui D, et al. Design and operation of reconfigurable two-dimensional DNA molecular arrays. Nat Protoc 2018;13(10):2312–29.
[30] Hong CA, Eltoukhy AA, Lee H, Langer R, Anderson DG, Nam YS. Dendrimeric siRNA for Efficient Gene Silencing. Angew Chem Int Ed 2015;54(23):6740–4.
[31] Barad O, Meiri E, Avniel A, Aharonov R, Barzilai A, Bentwich I, et al. MicroRNA expression detected by oligonucleotide microarrays: System establishment and expression profiling in human tissues. Genome Res 2004;14(12):2486–94.
[32] Ren K, Wu R, Karunanayake Mudiyanselage APKK, Yu Q, Zhao B, Xie Y, et al. In Situ Genetically Cascaded Amplification for Imaging RNA Subcellular Locations. J Am Chem Soc 2020;142(6):2968–74.
[33] Xue C, Zhang SX, Ouyang CH, Chang D, Salena BJ, Li Y, et al. Target-Induced Catalytic Assembly of Y-Shaped DNA and Its Application for In Situ Imaging of MicroRNAs. Angew Chem Int Ed 2018;57:9739–43.
[34] Chandrasekaran AR. Nuclease resistance of DNA nanostructures. Nat Rev Chem 2021::1–15.
[35] Li JJ, Geyer R, Tan W. Using molecular beacons as a sensitive fluorescence assay for enzymatic cleavage of single-stranded DNA. Nucleic Acids Res 2000;28:e52.
[36] Chandrasekaran AR, Vilcapoma J, Dey P, Wong-Deyrup SW, Dey BK, Halvorsen K. Exceptional Nuclease Resistance of Paranemic Crossover (PX) DNA and Crossover-Dependent Biostability of DNA Motifs. J Am Chem Soc 2020;142(14):6814–21.
[37] Gao Y, Li Q, Zhang J, Wu C, Shen Z, Xue C, et al. Bead-String-Shaped DNA Nanowires with Intrinsic Structural Advantages and Their Potential for Biomedical Applications. ACS Appl Mater Interfaces 2020;12(3):3341–53.
[38] Sahay G, Querbes W, Alabi C, Eltoukhy A, Sarkar S, Zurenko C, et al. Efficiency of siRNA delivery by lipid nanoparticles is limited by endocytic recycling. Nat Biotechnol 2013;31(7):653–8.
[39] Li S, Jiang Q, Liu S, Zhang Y, Tian Y, Song C, et al. A DNA nanorobot functions as a cancer therapeutic in response to a molecular trigger in vivo. Nat Biotechnol 2018;36(3):258–64.
[40] Li L, Tong R, Chu H, Wang W, Langer R, Kohane DS. Aptamer photoregulation in vivo. Proc Natl Acad Sci USA 2014;111(48):17099–103.
[41] Xu H, Gao J, Cai M, Chen J, Zhang Q, Li H, et al. Structural Mechanism Analysis of Orderly and Efficient Vesicle Transport by High-Resolution Imaging and Fluorescence Tracking. Anal Chem 2020;92(9):6555–63.
[42] Paddock SW. Principles and Practices of Laser Scanning Confocal Microscopy. Mol Biotechnol 2000;16(2):127–50.
[43] Lee H, Lytton-Jean AKR, Chen Yi, Love KT, Park AI, Karagiannis ED, et al. Molecularly self-assembled nucleic acid nanoparticles for targeted in vivo siRNA delivery. Nat Nanotechnol 2012;7(6):389–93.
[44] Shechter D, Harel M, Mukherjee A, Sagredo LM, Loven D, Prinz E, et al. Breast Cancer-Derived Microparticles Reduce Cancer Cell Adhesion, an Effect Augmented by Chemotherapy. Cells 2020;9(10):2269. doi: https://doi.org/10.3390/cells9102269.
[45] Li C, Xue C, Wang J, Luo M, Shen Z, Wu Z-S. Oriented Tetrahedron-Mediated Protection of Catalytic DNA Molecular-Scale Detector against in Vivo Degradation for Intracellular miRNA Detection. Anal Chem 2019;91(18):11529–36.
[46] Xu X, Yu S, Sun W, Qin X, Chen Y, Zhou L, et al. MiRNA signature predicts the response of patients with advanced lung adenocarcinoma to platinum-based treatment. J Cancer Res Clin Oncol 2018;144(3):431–8.
[47] Zeng C-W, Zhang X-J, Lin K-Y, Ye H, Feng S-Y, Zhang H, et al. Camptothecin induces apoptosis in cancer cells via microRNA-125b-mediated mitochondrial pathways. Mol Pharmacol 2012;81(4):578–86.
[48] Liu X, Li J, Cadilha BL, Markota A, Voigt C, Huang Z, et al. Epithelial-type systemic breast carcinoma cells with a restricted mesenchymal transition are a major source of metastasis. Sci Adv 2019;5(6):eaav4275. doi: https://doi.org/10.1126/sciadv.aav4275.
[49] Poudineh M, Sargent EH, Pantel K, Kelley SO. Profiling circulating tumour cells and other biomarkers of invasive cancers. Nat Biomed Eng 2018;2(2):72–84.